Scanning Microscopy

Volume 3 | Number 1 Article 9

11-14-1988

Complementary Surface Characterization of Chalcopyrite by Electron Microscopy, Electron Spectroscopy, and Optical Reflectance

P. H. Ruzakowski
University of Florida

P. H. Holloway
University of Florida

G. Remond
Bureau de Recherches Geologiques et Minieres

Scanning Microscopy, Vol. 3, No. 1, 1989 (Pages 71-82) 0891-7035/89$3.00+.00
Scanning Microscopy International, Chicago (AMF O'Hare), IL 60666 USA

COMPLEMENTARY SURFACE CHARACTERIZATION OF CHALCOPYRITE BY ELECTRON MICROSCOPY, ELECTRON SPECTROSCOPY, AND OPTICAL REFLECTANCE

P. H. Ruzakowski,* P. H. Holloway,*§ and G. Remond**

*University of Florida, Department of Materials Science and Engineering
Gainesville, Florida, 32611, U.S.A.
**Bureau de Recherches Geologiques et Minieres,
Departement Mineralogie-Geochimie-Analyses, 45060, Orleans Cedex, France

(Received for publication February 16, 1988, and in revised form November 14, 1988)

Abstract

Surface oxidation of polished natural specimens of chalcopyrite ($CuFeS_2$) at temperature between 23°C and 300°C in air has been characterized by Auger electron and X-ray photoelectron spectroscopies. The reaction products consisted of an outer iron oxide layer and an intermediate copper rich sulfide layer. Several different oxides and sulfides were consistent with the electron spectroscopy data, so specimens were analyzed as a function of time and temperature at selected 20 μm diameter areas with an optical microreflectometer (OMR). Since the optical properties of a compound are unique, a reflectance model with three homogeneous layers was used to calculate reflectance curves by varying the compound in and thickness of each layer. The reaction products were modelled as Cu_5FeS_4 in contact with the $CuFeS_2$ and Cu_2S as an intermediate layer between Cu_5FeS_4 and the outer oxide. The outer oxide was most consistent with Fe_3O_4. Relative layer thicknesses were calculated from a series of balanced chemical equations, and Cu_5FeS_4 was much thicker than Cu_2S with total thickness increasing with increasing temperature. The total film layer thicknesses calculated at 23°C were between 10nm and 35nm. At 200°C the film thickness varied from 8nm to 51nm with greater thicknesses associated with longer reaction times. Thicknesses at 300°C ranged from 12nm to 85nm.

KEY WORDS: Auger electron spectroscopy, X-ray photoelectron spectroscopy, optical microreflectometry, iron oxides, sulfides, surface oxidation.

§Address for correspondence:
Paul H. Holloway,
University of Florida,
Dept. Materials Science and Engineering,
Gainesville, FL 32611
Phone No. 904 392 1461

Introduction

Auger electron spectroscopy (AES) is a surface sensitive analytical technique with high spatial resolution that is routinely used to characterize the products at the surface of a material. Often bulk analytical techniques such as X-ray spectrometry using the electron probe microanalyzer (EPMA) are used in conjunction with surface sensitive techniques to study the role of the bulk composition on surface products or the elements concentrated at the surface and the trace elements present in the bulk [50,51]. For most materials these techniques are sufficient to characterize surface reaction products. However, in order to study the surface reaction products of minerals the spatial resolution of the technique is important due to the many phases present in natural ore mineral specimens. Optical reflectance is commonly used in mineralogy to identify the phases present in polished sections. High spatial resolution (20μm diameter or less) is made possible by focusing the incident monochromatic light and measuring the reflected intensity with a microscope from the specimen with a technique called Optical microreflectometry (OMR).

It is important first to characterize the minerals present in the bulk ore and any trace elements with EPMA and then to determine the surface products present. These products can be characterized by their optical properties and chemical composition with Auger electron spectroscopy (AES) over small areas routinely found in natural ore samples. The spatial resolution of the technique is important when studying minerals since the large area of analysis from XPS (typically ~5 mm but as small as 100 μm) as compared to that of AES (200 to 50 nm) and OMR (20 μm) can limit the relevance of the data. The chemical state information obtained with XPS from the surface compounds can be used to complement the surface elements detected with AES. Bulk elemental analysis is most commonly determined with EPMA with a lateral resolution of 10^3 nm or less. In addition EPMA has been used to analyze thin

films (as thin as 3nm) deposited on substrates [49]. Since EPMA has been mainly used as a bulk sensitive technique it can complement AES, XPS, and OMR data.

The complementary use of AES and OMR in characterizing the reaction products formed on chalcopyrite at temperatures between 23° and 300° will be demonstrated. Chalcopyrite, $CuFeS_2$, is a member of the sulfide family and is the main ore from which copper is extracted and is thus very valuable. In general, bulk mineral samples have a number of phases present which are often found as veins or large inclusions. The surface analytical techniques mentioned above lend themselves ideally to the study of surface oxidation of small areas present within naturally occurring sulfide minerals. The surface oxidation of chalcopyrite can affect further processing stages, in the recovery of copper, of the ore mineral and is thus important to characterize from the standpoint of mineral processing or beneficiation.

Literature Review

Electron spectroscopic techniques have been routinely used to analyze the surface and near-surface regions of solids since the early 1970's [33,46]. The application of these surface analytical techniques include the analyses of thin film products, with the characteristics of good depth resolution in XPS and AES, chemical state information from XPS, and high spatial resolution in AES. Bulk composition and trace element analysis is obtained from electron probe microanalysis (EPMA), whereas depth profiling is used in both AES and XPS [54] to characterize the composition of thin films. In general, information from AES and XPS are used in a semi-quantitative manner due to both instrumental and experimental limitations. These limitations can be controlled to some degree with standards, calibration techniques, and technological advances; however, it is important to understand the limits to these corrections. The complementary use of other surface analytical techniques in conjunction with AES and XPS should not be underestimated, specifically the use of a non-destructive optical technique such as optical microreflectometry (OMR).

The general theory of AES, XPS, and OMR are presented in the section on samples and experimental techniques. The most common uses of AES [17] include compositional analysis of the outer to near-surface region (0-3nm) for all elements except H and He and depth compositional profiling. The high spatial resolution capable with AES can be used to determine compositional variations across a surface with special emphasis on grain boundary and other interface analyses. Moreover, some chemical information can be obtained by analyzing energy shifts and the shape of the Auger signal [38]. The most common uses of XPS include surface analysis of all elements with the exception of H [45] and the acquisition of surface compositional analysis when the destructive effects of electron beam techniques must be avoided. In addition to these, one can include the chemical state identification of surface species [19,54], in-depth composition profiles of the elemental distribution in thin films [5,6,7,11], and the use of angle resolved XPS analysis for non-destructive depth analysis [9,14]. Unlike AES and XPS, OMR analysis does not require a vacuum and has been typically used to optically identify phases in bulk minerals [8]. Recently OMR [48] has been used to characterize the reaction products found on bulk sulfide minerals with the use of a reflectance model which will be described in the technique section.

Semiconductors [57], oxides [54,56,59], and sulfides [36,37] have been studied with AES in addition to metals and their alloys due to their importance in the electronics industry. The use of Auger data to obtain information about the measured electrical characteristics of semiconductor-metal contacts [57] has shown that in some systems, for example, in a silicide, the reaction due to heat treatment can be monitored. However, in other cases there is little correlation between the electrical characteristics and Auger depth profile data. Aluminum oxide films both deposited and grown on a substrate have been successfully analyzed with AES [54,59]. The use of AES to distinguish between different iron oxides formed on iron in gaseous and aqueous environments has been demonstrated [56] by using the peak to peak heights of the oxygen (510 eV) and iron (703 eV) lines and the fine structure of the low energy iron line (53 eV). Sulfides and their reaction products have also been studied with AES to better characterize the small phases present within a bulk mineral through the use of high spatial resolution AES [36,37]. Similarly, XPS has been used to study oxides [19,41], sulfides [5,6,7], and semiconductors [35]. Iron oxides have been characterized with XPS through mathematical deconvolution of the core line for a number of iron oxide compounds [19,41]. A number of sulfide minerals have been studied by combining XPS and electrochemical techniques to characterize the film products formed on the surface of natural bulk minerals [5,6,7]. The oxidation state of semiconductors have also been studied as in the case of the different oxidation states for copper oxide grown on a copper substrate [35]. Iron oxide film layers have been characterized with OMR through the use of optical constants and in combination with AES depth profiling analysis [48].

A number of factors can affect the quantification of Auger and XPS analysis. For example, backscattering effects [16,58] in AES analysis, surface morphology [27] effects mainly in AES, charging of insulators [22,44] in both AES and XPS, electron-beam induced artifacts [25,31,42,43] in AES, and ion-beam induced artifacts [39,53] during sputtering in both AES and XPS. Backscattered electrons [16,58] result in the emission of Auger electrons in addition to those produced by the primary electrons which can lead to erroneous interpretation of the data. The backscattering effect is dependent upon the primary electron beam energy and the composition of the specimen. A set of elements spanning a large range of Z values were used to

show that the backscattering effect increased with atomic number Z and primary energy [58]. The film thickness of a material on a substrate can result in a backscattering effect which can also affect the Auger electron yield [16]. Similarly a number of restrictions are placed on the specimen used for analysis with OMR. The specimen must be flat and mounted perpendicular to the optical axis during analysis. In addition the optical constants used for the film during the modelling calculations are assumed to be the same as the bulk constants as is commonly done in ellipsometry.

The original surface topography or morphology can affect not only the Auger electron yield [27] but can also influence the depth resolution [24,63] which leads to increased interface broadening with sputter depth. Surface roughness was found to affect quantitative AES analysis independent of whether absolute peak to peak heights or relative peak heights are used [27]. Thus, the initial surface morphology must be considered during rigorous quantitative Auger analysis to determine the validity of data interpretation. Surface roughness effects in XPS will in general reduce the surface sensitivity enhancement at low grazing angles [14] from one point to another across a specimen's surface. In addition certain regions on the surface may be shaded from other regions by adjacent raised areas at a given grazing incidence. Quantitative analysis of grazing-incidence data can be affected by the surface roughness for very low grazing angles due to the change that occurs in the degree of refraction and reflection for a small change in angle of incidence at low grazing-incidence analysis. In general, surface roughness effects in OMR decrease the overall intensity of the reflectance curve (wavelength versus intensity) obtained from the surface. For very rough surfaces there may be a wavelength dependence [1,32,47], however, in this study the polishing procedure in the last 2 stages did not affect the overall intensity of the reflectance curve.

Since many of the materials analyzed with AES have an oxide film on the surface through either deliberate preparation or surface oxidation there is a possible charging problem during Auger analysis [44]. These insulators tend to accumulate charge on their surface during both Auger electron and X-ray photoelectron analysis [46] due to their high resistance. When charge accumulates on insulators the resulting electric field may cause diffusion of mobile ions. This was shown to occur [44] for Na ions in soda-lime-silicate glasses under Auger analysis. It has been shown that the problem is one of diffusion [43] where both mobility and driving force are affected by ion or electron irradiation in Auger analysis. The accumulated charge affects the driving force for diffusion, while beam heating increases the ionic mobility. Sample charging during Auger analysis can be reduced by mounting the sample at a 30° angle. For very thick insulating structures this may not be enough to reduce the surface charge. Lowering the current density has also been effective in reducing the surface charge. Sample charging in XPS influences the ionization energies. If there is an induced surface potential then the energy required to ionize an electron is increased by an amount proportional to the surface potential. This affects the accurate measurement of electron binding energies in solids. In addition ionization energies must be corrected for the spectrometer work function which includes instrumental terms that affect the electron kinetic energy scale. This term is generally determined in a calibration process with a material of known ionization energies from an independent source.

In addition to the effect of a specimen's surface preparation on the Auger signal intensity it is also possible for the sample to change during analysis due to interaction of the primary electron beam with the specimen. Electron beam artifacts resulting from the interaction of the electron beam with the sample can include [40] adsorption of residual gases, desorption of surface species, migration of mobile species, heating of the sample, sample charging, and molecular cracking.

Auger electron and X-ray photoelectron spectroscopy are often used as a surface atom removal technique (sputtering) to measure the composition at the surface and through a film. This process can result in a number of sputtering artifacts. These can include surface roughening [64], knock-on effects [21,64], and preferential sputtering [21,64]. Induced surface roughness can change the Auger signal strength [27] and thereby affect the absolute and quantitative Auger analysis. Even in the case of a flat amorphous surface cone formation may develop under ion bombardment due to the angle dependence of the sputtering yield. Knock-on effects can cause broadening of depth profiles due to a collisional cascade buildup where the primary recoils are forced into deeper layers [23]. Preferential sputtering can result in different sputtering yields of two elements in a binary alloy which results in a change in the surface concentration of a sputtered sample. For a Cu-Ni (50 weight percent) sample surface or a sputter-deposited layer on a substrate it has been shown [53] that there is an enrichment in Ni at the surface. The influence of ion bombardment (sputtering) in XPS is similar to that of AES. Sputtering may result in the reduction of metal oxides [30,61] and may also result in the formation of new compounds.

Samples and Experimental Techniques

Sample Origin And Preparation

Mineral Origin. The bulk chalcopyrite specimens used in this study originated from two distinct deposits. The Le Burc deposit in Tarn, France made up the majority of the samples used in this study. Two other phases, covellite (CuS) and goethite (FeOOH or $HFeO_2$), were present as veins (or inclusions) within the chalcopyrite matrix. Additionally, gangue, a component consisting mainly of silicates was present. Le Burc specimens free of inclusions or veins of copper sulfides and iron oxides were

used for comparison with specimens with inclusions in this study.

The second source of chalcopyrite specimens used in this study originated from Butte, Montana, USA. These specimens contained veins of chalcocite (Cu_2S) and goethite as well as gangue material within the bulk chalcopyrite. All available specimens from the Butte mine contained inclusions. In some cases specimens with only Cu_2S inclusions were used to study the effect of temperature on the inclusion.

Sample Preparation. Samples were first cut with a Buehler diamond saw to sizes ranging from 5mm x 5mm to 6mm x 10mm and then hand polished. Hand polishing the specimens decreased the overall temperature effect which results from automatic polishing wheels. The polishing process utilized dry silicon carbide paper starting with 180 grit, then changing to 320 grit and finishing with 600 grit. The samples were ultrasonically cleaned in reagent grade petroleum ether for 10 minutes between each polishing stage to eliminate stray particles which could scratch the surface in a subsequent grinding stage. After the dry grinding steps the next stage consisted of diamond polishing the specimens (hand polishing) in an extender consisting of equivalent proportions of mineral oil and kerosene [34]. The specimens were cleaned between polishing stages as described above. The diamond polishing compounds were obtained from Buehler. Polishing was started with 15μm diamond paste and went through 6μm, 1μm, and finished with 0.25μm diamond. The polishing times were longest for the 15μm and 6μm stage (approximately 10 minutes) and decreased for the 1μm stage to 5 minutes and approximately 2 to 3 minutes for the 0.25 μm stage. The surface of the polished specimens were checked periodically with a microscope for scratches between polishing stages to optimize the overall polishing process.

Samples were stored before and after polishing in laboratory air. The relative humidity ranged between 45% and 70%. The temperature ranged between 20°C and 26°C. Chalcopyrite samples and bulk materials were stored in plastic containers under the above conditions. Samples were always handled with tweezers or plastic gloves after polishing or other treatments.

Auger Electron Spectroscopy (AES)

A Perkin Elmer Model 600 Scanning Auger Multiprobe (SAM) or a Perkin Elmer Model 660 recently installed in the Department of Materials Science and Engineering at the University of Florida was used to analyze the surface of chalcopyrite specimens. Specifically, AES [26,55] has been used to study the spatial distribution of specific elements over the surface and their variation with depth into the solid. It is also being used to study semiconductors, metals, alloys and mineralogy to study the outer surface layers for contamination, surface migration, or segregation, as well as diffusion studies (often in conjunction with a number of surface analytical techniques) [4,18,28,56,62].

The primary electron beam energy in this study was generally 5keV with a beam current of 0.050μA. The base pressure of the vacuum system was typically 5×10^{-10} Torr. Secondary electron images are used to help locate the specific areas of interest on a specimen. The electron spectrometer in SAM was a cylindrical mirror analyzer. A 3keV argon ion gun with a current density of $25mA/mm^2$ and a raster size of 3x3mm was used for sputter removal of atoms from the sample surface. The gun was operated with an argon pressure of 5×10^{-5}Torr.

Optical Microreflectometry (OMR)

The reflectance technique used in this study to optically characterize freshly polished surfaces and thin films formed on these surfaces is called optical microreflectometry (OMR). Traditionally reflectometry has been used in mineralogy to identify small phases present within an ore mineral. Experimental reflectance curves were measured with normally incident light between 420nm and 740nm. The optical microreflectometer (see Figure 1) was further developed by Caye [8] in its present use. There are four main components (see Figure 1): (1) a white light source, (2) a monochromator (see Figure 1), (3) the microscope and (4) a detector. White light from the source is monochromatized and focused onto a sample by the microscope (20X objective, 0.4 numerical aperture). The area of analysis was 20μm in diameter. The reflected light is also focused by the microscope and its intensity is measured by the photomultiplier tube. The result is a reflectance curve (i.e., a plot of percent reflectance versus wavelength). A standard (SiC) is generally used to determine the reflectance of an unknown specimen, R_{spec} by,

$$R_{spec} = R_{stan} \ (I_{spec})/(I_{stan}) \qquad (1)$$

where I_{spec} or I_{stan} represents the reflected intensity from either the specimen or the standard, respectively, and R_{stan} is the known reflectance of the standard. The reflectance curve for a bulk homogeneous solid may also be calculated using the complex index of refraction (see equations 2 and 3 below). Although more

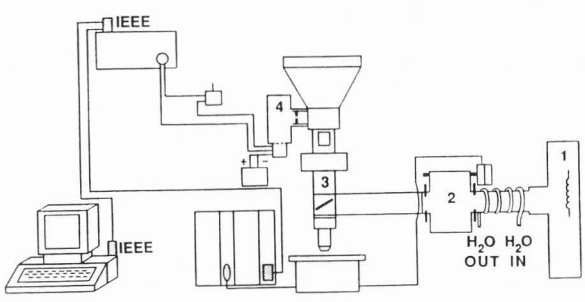

Figure 1. Schematic diagram of the Optical microreflectometer used to measure the percent reflectance as a function of wavelength between 420nm and 740nm. The numbered components are 1) white light source, 2) monochromator, 3) microscope and 4) photodetector.

complicated, a reflectance model was developed to calculate reflectance curves for a bulk solid covered with a thin absorbing layer of a different chemical compound [48].

This model assumes normally incident light onto an absorbing substrate covered with one or more thin absorbing films. The substrate and films are assumed to exist with perfectly parallel interfaces [48]. Bulk optical constants have been used for the films in calculating the reflectance curves. Development of the model starts with the interaction between substrate i and air k. The reflectance coefficient between medium i and k is given by:

$$R_{ik} = \frac{(n_i - n_k)^2 + (x_i - x_k)^2}{(n_i + n_k)^2 + (x_i + x_k)^2} \qquad (2)$$

where n is the real refractive index and x is the extinction coefficient. The optical constants n and x are related to the complex index of refraction N, by $N = n - j\,x$. The phase change Θ_{ik} of light reflected at the interface is given by:

$$\tan(\Theta_{ik}) = \frac{2(n_i x_k - n_k x_i)}{(n_i^2 - n_k^2) + (x_i^2 - x_k^2)} \qquad (3)$$

Equations 2 and 3 may be extended to a substrate covered with a thin film in contact with air. Reflection at both interfaces plus multiple internal reflections within the single homogeneous layer is traced and the photodetector detects the intensity of the amplitudes of the reflected wave which are summed. An overall phase change can be described which includes phase changes due to reflection at successive interfaces and the phase changes due to optical path difference. The resulting reflected intensity from a substrate (0) covered with an absorbing thin layer (1) in contact with air (2) is denoted as R' where d is the thickness of the film and L is the wavelength of light

(4)

$$R' = \frac{R_{21} + R_{10}e^{2A} + 2\{R_{21}R_{10}\}^{.5}e^{A}\cos\{\Theta_{21}\Theta_{10} + 4\pi n_1 d_1/L\}}{1 + R_{21}R_{10}e^{2A} + 2\{R_{21}R_{10}\}^{.5}e^{A}\cos\{\Theta_{21} + \Theta_{10} - 4\pi nd/L\}}$$

where $A = -4\pi x_1 d_1/L$.

Thus, for a single homogeneous layer, the resulting reflectance, R', is a function of the phase changes at each interface Θ_{ik}, the reflection from each interface, R_{ik}, the optical constants n and x, the film thickness d, and the wavelength of light, L. This model can be extended to multiple thin films on a substrate through an iterative procedure [48]. For this study three homogeneous layers were used to model the reaction products formed on chalcopyrite.

Electron Probe Microanalyzer (EPMA)

X-ray spectrometry using the Electron probe microanalyzer for mineral analysis has been described previously [51]. The equipment is installed in the joint BRGM-CNRS laboratory in Orleans, France. It is fully computer automated with four wavelength dispersive X-ray spectrometers. The experimental data were converted to weight concentrations by the use of the ZAF analytical expression [20]. In general this technique was used to characterize the bulk composition of chalcopyrite and other phases present within the specimen. Data from EPMA showed that arsenic, silver, selenium, and indium were below the detection limits of 270ppm, 500ppm, 500ppm, and 850ppm, respectively, in the bulk chalcopyrite specimens.

X-ray photoelectron spectroscopy (XPS)

A Kratos XSAM 800 X-ray Photoelectron spectrometer (XPS) installed in the Department of Materials Science and Engineering at the University of Florida was used to further complement the AES and OMR data. Chemical state information on the products formed on the surface of $CuFeS_2$ and as a function of film depth was obtained [52]. Angle resolved or grazing angle XPS was used to increase the sensitivity to species at the surface [2]. As the angle of electron emission relative to the sample surface is decreased, the surface area analyzed is increased while the sample depth analyzed is decreased; this has the effect of increasing the relative peak intensities of the surface species. An angle of 90° was used for normal analysis while a grazing angle of 25° was used for angle resolved analysis. The use of this technique was limited by the spatial resolution as compared to AES and OMR.

Results and Discussion

The inclusions present in the bulk chalcopyrite specimen are shown in the photo in Figure 2. A secondary electron image of a specimen with a copper sulfide inclusion is shown in Figure 2a, the white area is chalcocite (Cu_2S) while the dark area is the bulk chalcopyrite. A backscattered electron image is shown in Figure 2b for another bulk chalcopyrite specimen with bornite (Cu_5FeS_4) and goethite (FeOOH) inclusions. The dark grey areas represent the goethite regions while the light grey areas represent the bornite inclusions with the remaining area the bulk chalcopyrite. Due to the presence of inclusions throughout the specimen it was necessary to use Auger electron spectroscopy in the point analysis mode.

Auger electron spectra

Auger point analysis on the chalcopyrite area of the specimen was employed to obtain a depth profile of the film formed after heat treatment at 300°C. The color associated with this specimen was orange-pink as compared to the

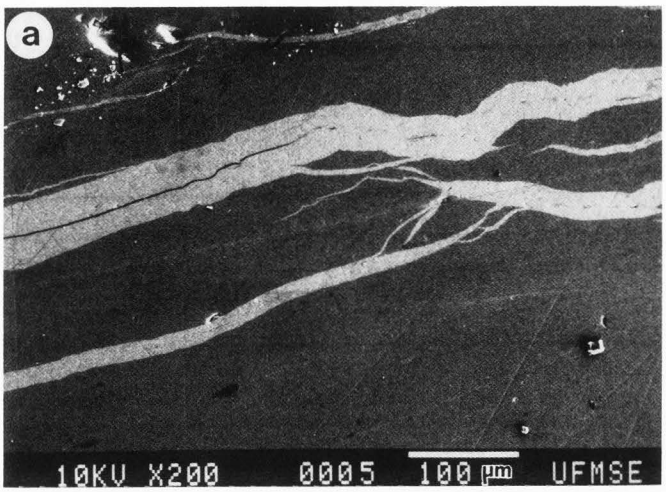

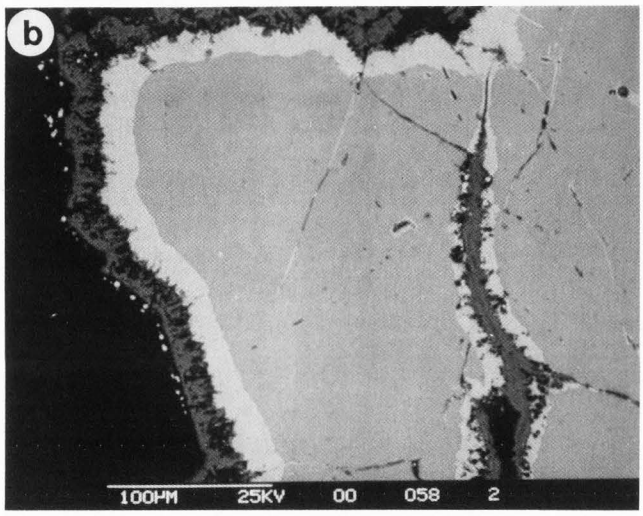

Figure 2. Secondary and Backscattered electron images of chalcopyrite specimens; a) secondary electron image of chalcopyrite with chalcocite inclusions (as white veins) and b) backscattered electron images of bulk chalcopyrite with bornite inclusions (light grey veins) and goethite (dark grey veins). Bars = 100 µm (in both figures).

brass-yellow of the freshly polished specimen. Color formation has been correlated with film thickness [29] and impurities reacting to form a compound at the surface of chalcopyrite [10] both in the bulk and from adjacent minerals found in contact with chalcopyrite. Auger spectra (Figure 3) of the chalcopyrite region showed that the primary chemical constituents detected on the surface were Fe and O with some C and S. Additionally, two low energy Fe MVV transitions were detected before sputtering (Figure 3a). The low energy Fe MVV transition (48.0eV) initially showed the presence of an iron oxide because the Fe MVV transition was split into two peaks at 45.0eV and 51.0eV (peak energy difference equals 6.0eV). The split in peaks and the energy difference between the two peaks is consistent with an Fe_3O_4 layer with a small amount of Fe_2O_3 or FeOOH (increases the peak energy difference) at the surface [56]. Dry oxidation of chalcopyrite [12] was studied with Auger electron spectroscopy (AES). Initial adsorption of oxygen was associated with Fe rather than Cu as demonstrated by the fact that the low energy Fe MVV peak at 47eV split into two peaks at 49eV and 40eV (C was at 269eV). These two Fe peaks have been associated with Fe_2O_3 and oxidized iron surfaces, that is, they appear to be associated with the formation of Fe^{+3}. The total thickness of the oxidation layer after 30 minutes' exposure in dry air was 1.2nm. Results [12] from naturally weathered pieces of chalcopyrite (utilizing AES depth profiling) found film layers that were much thicker and varied between samples. The variation was not described although it was implied as a difference in the total thickness of the film layers.

From XPS data the FeOOH layer is believed to be present with the Fe_3O_4. Sputtering resulted in a decrease in the peak energy difference to 5.0eV which is consistent with Fe_3O_4 [56] and sputter removal of FeOOH. After depth profiling (Figure 3b), only one Fe MVV transition was detected. The splitting of the Fe MVV Auger transition upon oxidation has been interpreted in terms of a cross transition between the O 2p states and the Fe 3p states in Fe_3O_4 [13]. That is, the emergence of two new peaks in the Auger spectrum is associated with rearrangement of the electronic structure of the valence band due to oxide formation.

The depth profile for the chalcopyrite region (see Figure 3c) showing an outer oxide layer was observed. A copper-rich sulfide layer, with copper in the same oxidation state as the bulk, between the oxide and the bulk chalcopyrite was indicated (approximately 4 minutes of sputtering) since the Cu/Fe peak to peak ratio is greater than unity.

In another study [3] chalcopyrite was exposed to air and then characterized with XPS. Exposure of chalcopyrite to air caused a rapid formation of iron hydroxide or oxyhydroxide within the first few layers. Basic iron sulfate ($Fe_2(SO_4)_3$) was formed subsequently and was stated to be the major oxidation product in air. The copper was found to remain in the same chemical state (Cu^{+1}) as found in the bulk by monitoring the x-ray induced Cu L_3VV line and the Cu(2p(3/2)) line as a function of reaction time (30days) in air. Exposure to air was not found to involve the formation of ferric sulfate ($FeSO_4$) or sulfur (S) in the first few layers of oxidation. The detection of an iron oxide and a sulfate is consistent with the present study however the iron oxide is the predominant surface reaction product in this study. It must be noted that the specimen from Brion's work was in powder form and contained other mineral phases present while the present study used polished bulk surfaces.

The copper-rich region and the iron oxide region near the surface may have a region in between but this could not be clearly detected

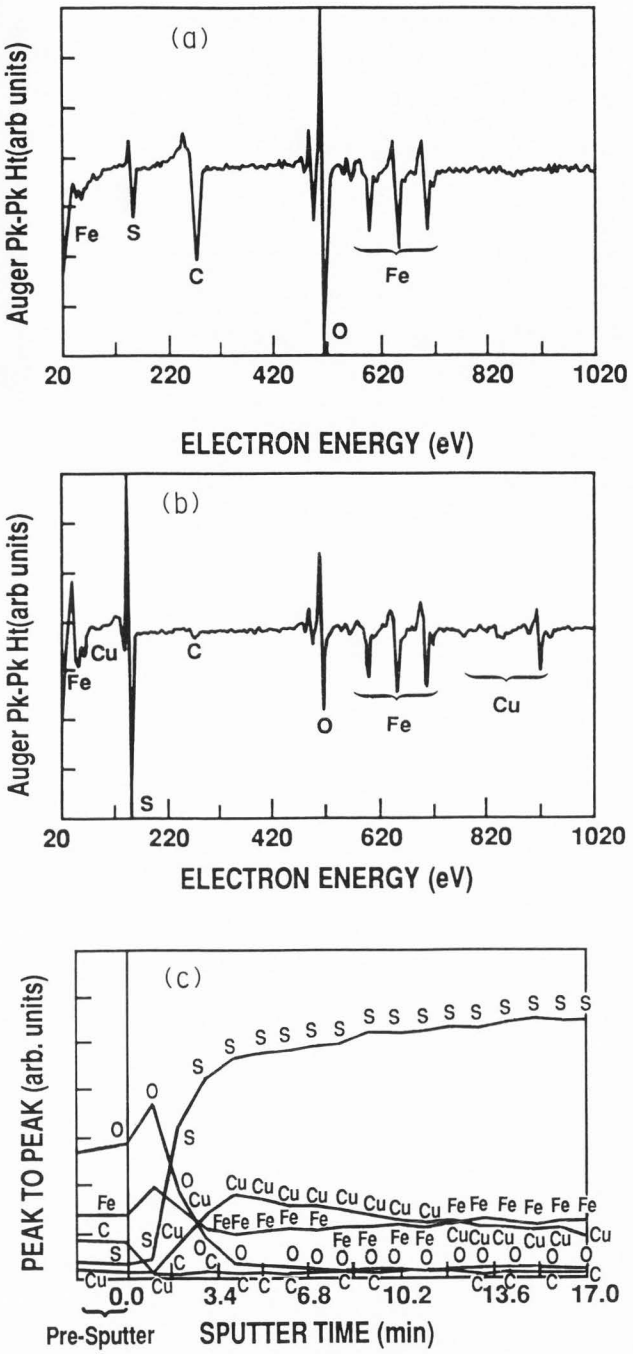

Figure 3. AES point analysis for a chalcopyrite (heated 300°C, 1h) area in a bulk natural specimen; a) survey scan before sputtering, b) survey scan after 17 minutes ion sputtering, and c) depth profile.

by AES. Thicker iron oxide layers with increased heating at 200°C and 300°C was observed. This was also consistent with the data obtained from the reaction at 23°C as a function of time.

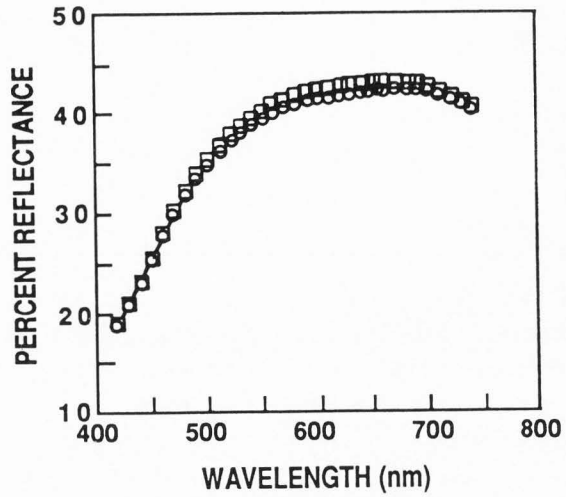

Figure 4. Reflectance curves from natural bulk chalcopyrite specimens measured immediately after polishing (data from two different samples shown to demonstrate reproducibility).

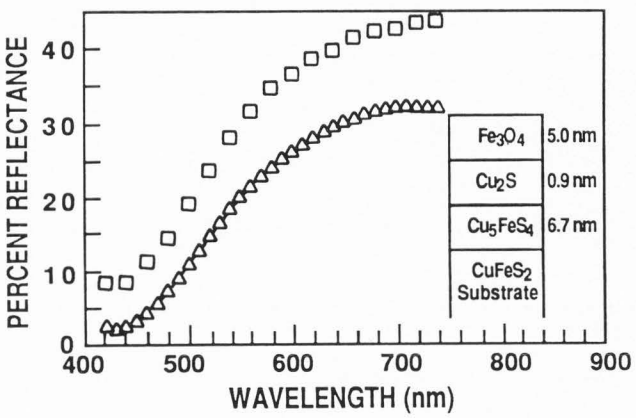

Figure 5. Experimental (Δ-Δ) reflectance curve for chalcopyrite reacted in air at 23°C for 1.5 years versus a calculated (□) reflectance curve for the film geometry with reaction products as shown in the schematic next to the reflectance curves.

Optical microreflectometry (OMR)

To better characterize the reaction products in terms of their spatial geometry and the compounds present reflectance curves were obtained from specimens after heat treatment or long time reaction in air (9 months to 1.5 years). The area of analysis complemented the area analyzed with AES. In fact, reflectance curves were obtained prior to obtaining data from AES and before and after heat treatment.

Reflectance curves for freshly polished samples from chalcopyrite areas within the bulk specimen are shown in Figure 4. This curve can be compared with the reflectance curve shown in Figure 5 for a specimen reacted at 23°C for 1.5 years (triangles). A minimum in percent reflectance at 430nm is observed.

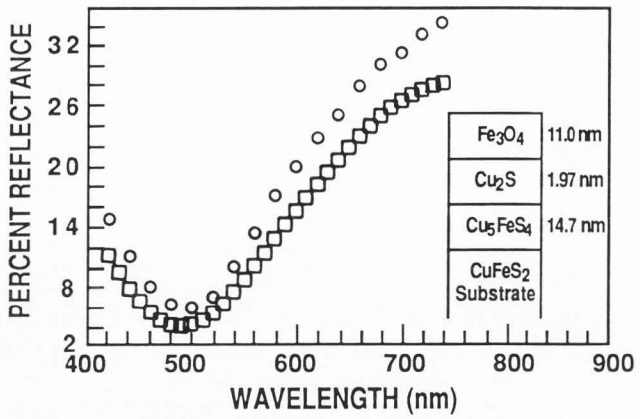

Figure 6. Experimental (▫-▫) reflectance curve for chalcopyrite heated in air at 300°C for 1h versus a calculated (o) reflectance curve for the film geometry with reaction products as shown in the schematic next to the reflectance curves.

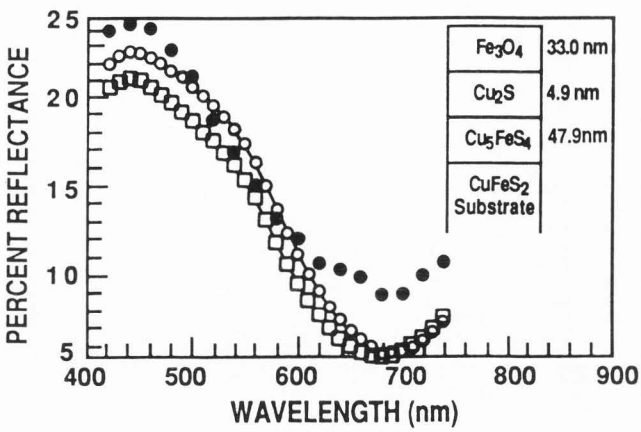

Figure 7. Experimental reflectance curves from two different points (▫-▫, o-o) for chalcopyrite reacted in air at 300°C for 2h versus a calculated reflectance curve (•) for the film geometry with reaction products as shown in the schematic next to the reflectance curves.

This minimum in percent reflectance at a specific wavelength will be designated as L_{min}. The calculated reflectance curve is also shown in Figure 5 (squares) for an outer magnetite layer an inner bornite layer in contact with the chalcopyrite and an intermediate layer of chalcocite between the magnetite and the bornite. The reflectance curves of chalcopyrite areas in the bulk specimens at 200°C and 300°C were equivalent to those reported at 23°C. A sequential shift in L_{min} to longer wavelengths was observed with an increased thickness in the outer magnetite layer as shown in Figure 6 and Figure 7 for L_{min}= 490nm and 695nm, respectively. In addition to the shift to longer wavelengths a broad peak was observed at 440nm as shown in Figure 7. The shift in L_{min} is associated with both the increase in iron oxide thickness and the optically absorbing properties of the compounds formed at the surface.

Based on the surface products reported from the literature in both aqueous and nonaqueous environments a number of film geometries were postulated as an initial attempt to calculate reflectance curves. As a first attempt the intermediate region was chosen to be bornite, Cu_5FeS_4, while the outer oxide layer was varied between Fe_3O_4 (magnetite), Fe_2O_3(hematite), and FeOOH(goethite). Reflectance curves were calculated by first obtaining a curve for each appropriate crystallographic orientation for Fe_2O_3 and for FeOOH then averaging these reflectance curves to obtain a final reflectance curve for each compound. Chemical equations were written for chalcopyrite reacting with oxygen and in some cases reacting with water to form bornite and either magnetite, hematite, or goethite as the outer oxide. Sulfur dioxide was released as a gas. Roasting data [15,60] has shown that SO_2 is given off at temperatures of 500°C and above. Resistivity data from chalcopyrite [15] has shown that sulfur is released from the bulk substrate from below room temperature up to 310°C thus depleting the bulk composition in sulfur. Sulfur burns in air to form SO_2 which can be released as a reaction product both at 23°C, 200°C, and 300°C.

Chemical equations are first written and then balanced according to the number of moles on each side of the equation. Following this the density (Γ gm/cm^3) and molecular weight (MW) of each compound are used to calculate a thickness (D) of the compound formed assuming a unit area of reaction. In addition the amount of chalcopyrite that is consumed can also be calculated and checked to be sure that this is consistent with the specimen. It was found that the amount of chalcopyrite consumed was a small fraction of a percent of the thickness of the sample (e.g., 100nm consumed from a 4mm thick specimen corresponds to a thickness change of only 0.0025%).

An example of the calculation for chalcopyrite reacting to form bornite (Cu_5FeS_4) in contact with the chalcopyrite, plus an outer layer of Fe_3O_4, and a Cu_2S or CuS layer between the iron oxide and the bornite layer was shown in Figure 5 through Figure 7. The series of balanced chemical equations for this type of a film layer structure and the ratio of the film layer thicknesses of one layer to another are shown in Table 1. In this equation chalcopyrite reacted with oxygen to form a bornite layer, either a covellite or chalcocite layer, and an iron oxide. The iron oxide thicknesses were varied between 1nm and 33nm which set the thickness of the copper sulfide and the bornite layers. The first balanced chemical equation in Table 1 is for a Cu_2S layer while the second set is for a CuS layer.

Modelling the layer between bornite and the outer iron oxide as either CuS or Cu_2S both resulted in reasonable fits in most cases. This is partially due to reduced sensitivity since

the ratio of thickness of the iron oxide to the copper sulfide is 6.53 and 7.95 for Cu_2S and CuS, respectively. However, the majority of the curves were better fit with a Cu_2S layer. It is not possible to distinguish between covellite and chalcocite based upon either AES or XPS data. Although OMR data could not be used conclusively to determine which copper sulfide is present the reflectance modelling results suggest chalcocite, Cu_2S, to be the product formed most often. Moreover, the free energy of formation is 8kcal/mole more negative for Cu_2S than for CuS.

It is of interest to attempt to relate L_{min} to the thickness of the reaction layer. By comparing the shapes and percent reflectance of calculated and experimental curves, it was possible to extrapolate back to a film layer thickness and relate the L_{min} value to an average thickness for the outer oxide; of course, this in turn sets the thicknesses of the other two layers. A plot of L_{min} versus the average thickness of the outer iron oxide as shown in Figure 8, where data are shown for an Fe_3O_4 outer layer and either Cu_2S or CuS layer between the oxide and bornite. Obviously, the shift in L_{min} and thicknesses of the outer iron oxide layer are correlated. The observed slight curvature results from contributions from the other reaction products (Cu_2S, CuS, and Cu_5FeS_4) to the shift in L_{min} as they thicken. Even the thin Cu_xS layer can be important [52] since removal of the Cu_2S layer caused L_{min} to shift to a lower wavelength, even though the oxide layer thickness remained constant.

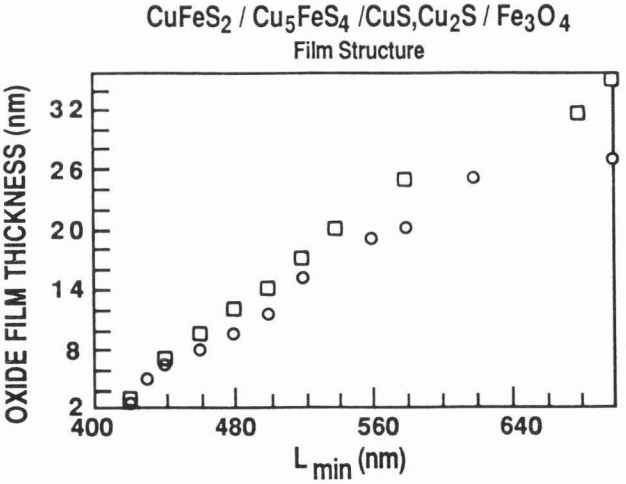

Figure 8. Iron oxide (magnetite) film thickness versus the shift in the wavelength minimum (L_{min}), assuming either CuS (□) or Cu_2S (o) is at the chalcopyrite/magnetic interface.

Thus, by combining AES and OMR data it was possible to characterize the reaction products formed on chalcopyrite between 23°C and 300°C. This data was also found to be consistent with XPS data which demonstrated that a thin iron hydroxide layer was present. In addition, a very thin layer of copper and iron sulfates were present (0.5 - 1.0nm). Depth profiling and angle resolved data demonstrated that the sulfate and the hydroxide were concentrated only at the surface while an iron oxide was found as a function of depth into the film. The presence of inclusions do not change the overall reaction of the bulk chalcopyrite for distances greater than 100μm from a chalcopyrite/inclusion interface.

Table 1. Chemical equations used to calculate thickness ratios between layers designated as bornite, chalcocite, covellite, and magnetite. The amount of bulk chalcopyrite consumed is designated as D_c.

Compound: Chalcopyrite/Bornite/Chalcocite/Iron Oxide

Formula: $CuFeS_2$ /Cu_5FeS_4/ Cu_2S / Fe_3O_4

Thickness: D_c D_b D_t D_f

$CuFeS_2 + 1.805O_2 \rightarrow 0.17\ Cu_5FeS_4 + 0.08\ Cu_2S + 0.28\ Fe_3O_4 + 1.25\ SO_2$

$D_b = 0.385\ D_c$; $D_f = 0.287\ D_c$; $D_t = 0.179\ D_f$

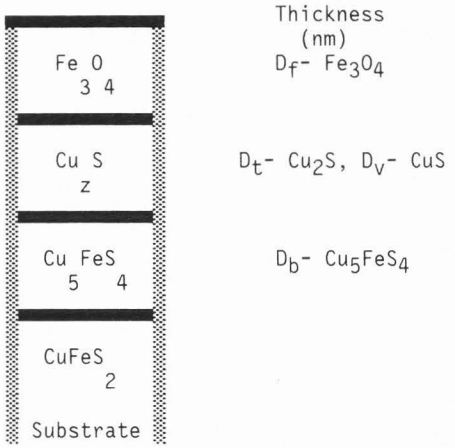

Compound: Chalcopyrite/ Bornite /Covellite/Iron Oxide

Formula: $CuFeS_2$ / Cu_5FeS_4/ CuS / Fe_xO_y

Thickness: D_c D_b D_v D_f

$CuFeS_2 + 1.73\ O_2 \rightarrow 0.18\ Cu_5FeS_4 + 0.09\ CuS + 0.27\ Fe_3O_4 + 1.18\ SO_4$

$D_b = 0.41\ D_c$; $D_v = 0.104\ D_b$; $D_f = 6.61\ D_v$

Summary

The characterization of the reaction products formed on bulk chalcopyrite as a function of temperature demonstrated the complementary use of AES and OMR. Depth profiling with AES detected an iron oxide (magnetite) and a copper-rich sulfide underlying layer over the bulk chalcopyrite. The spatial geometry and the compounds present were further characterized with OMR. Balanced chemical equations were used to calculate from OMR the relative thicknesses of the film layers. The film structure obtained by using both OMR and AES consisted of an outer magnetite layer with a bornite layer in contact with the bulk chalcopyrite and an intermediate Cu_xS layer between the magnetite and the bornite. It is postulated that the most likely intermediate layer product was chalcocite based on thermodynamic free energy of formation data. Thus, the balanced chemical equations allow a one parameter fit of the reflectance data. Data from XPS analysis confirmed the presence of an iron oxide on a macroscale and moreover detected a hydroxide and sulfate on the outer 0.5 to 1nm of the film. The backscattered and secondary electron images allow a specific area to be chosen which can then be analyzed at the same point with both AES and OMR.

References

1. Bennett CEG, Porteus JO (1961) Relation between surface roughness and specular reflectance at normal incidence. J. of the Optical Soc. of Amer. 51, 2, 123-129.

2. Briggs D, Seah MP (Eds.) (1983) Practical Surface Analysis by Auger and X-ray Photoelectron Spectroscopy, John Wiley and Sons, Ltd., New York, 1-533.

3. Brion D (1980) Etude par spectroscopie de photoelectrons de la degradation superficielle de FeS_2, $CuFeS_2$, ZnS et PbS a l'air et dans l'eau, Appl. of Surf. Sci. 5, 133-152.

4. Brundle CR (1974) The application of electron spectroscopy to surface studies. J. of Vac. Sci. and Technol. 11, 212-224.

5. Buckley AN, Hamilton IC, Woods R (1984) Investigation of the surface oxidation of bornite by linear potential sweep voltametry and X-ray photoelectron spectroscopy. J. of App. Electrochemistry, 14, 63-74.

6. Buckley AN, Woods R (1984) An X-ray photoelectron spectroscopic study of the oxidation of galena. Applications of Surf. Sci., 17, 410-414.

7. Buckley AN, Woods R (1984) An X-ray photoelectron spectroscopic study of the oxidation of chalcopyrite. Australian J. of Chem., 37, 2403-2413.

8. Caye R (1973) Contribution au developpement de la microreflectometrie sous incidence oblique pour l'etude de mineraux. These, Universite, Paris VI.

9. Chaney RL (1987) Recent developments in spatially resolved ESCA. Surf. and Interface Anal., 10, 36-47.

10. Chen TT, Dutrizac JE, Owens DR Laflamme JHG (1980) Accelerated tarnishing of some chalcopyrite and tennantite specimens. Can. Miner. 18, 173-180.

11. Connor JA (1978) XPS studies of Inorganic and Organometallic Compounds. In: Handbook of X-ray and Ultraviolet Photoelectron Spectroscopy, D. Briggs, (Ed). Heyden London, 183-209.

12. Eadington P (1977) Study of oxidation layers of surfaces of chalcopyrite by use of Auger electron spectroscopy. Trans. Inst. Min. Met. C., C86, 186-189.

13. Ertl G, Wandelt K (1975) Electron spectroscopic studies of clean and oxidized iron. Surf. Sci. 50, 479-492.

14. Fadley CS (1984) Angle-resolved X-ray photoelectron spectroscopy. Progress in Surf. Sci., 16, 275-388.

15. Frueh Jr. AJ (1959) The use of zone theory in problems of sulfide mineralogy, Part II; The resistivity of chalcopyrite. The Amer. Mineral. 44, 1010-1019.

16. Goto K, Ishikawa K, Koshikawa T, Shimizu R (1975) Auger and secondary electrons excited by backscattered electrons; An approach to quantitative analysis. Surf. Sci., 47, 477-494.

17. Haas TW, Pocker DJ (1974) Some applications of Auger electron spectroscopy to metallurgical problems. J. Vac. Sci. Technol. 11, 1087-1092.

18. Harris LA (1968) Analysis of materials by electron-excited Auger electrons. J. of Appl. Phys. 39, 1419-1427.

19. Hawn DD, Dekoven BM (1987) Deconvolution as a correction for photoelectron inelastic energy losses in the core lever XPS spectra of iron oxides. Surf. and Interface Anal., 10, 63-74.

20. Henoc J, Heinrich KFJ, Myklebust RL (1973) A rigourous correction procedure for quantitative electron probe microanalysis (COR 2), Nat. Bur. of Stand. Washington DC., (US), Tech. Note 769, 1-132.

21. Ho PS, Lewis JE, Wildman HS, Howard JK (1976) Auger Study of preferred sputtering on binary alloy surfaces. Surf. Sci. 57, 393-398.

22. Hofmann S (1979) Auger electron spectroscopy. In: Comprehensive Analytical Chemistry, Volume 9, Svehla G, (Ed)., Elsevier, Amsterdam, 89-172.

23. Hofmann S (1983) Depth Profiling. In: Practical Surface Analysis by Auger and X-ray Photoelectron Spectroscopy, Briggs D, Seah MP, (Eds). John Wiley and Sons, New York, 141-177.

24. Hofmann S, Erlewein J (1977) Depth resolution and surface roughness effects in sputter profiling of NiCr Multilayer sandwich samples using Auger electron spectroscopy. Thin Sol. Films, 43, 275-283.

25. Hofmann S, Zalar A (1979) Electron beam effects during the sputter profiling of thin Au/Ag films analyzed by Auger electron spectroscopy. Thin Sol. Films, 56, 337-342.

26. Holloway PH (1980) Fundamentals and applications of Auger electron spectroscopy. Adv. in Elec. and Electron Phys. 54, 241-298.

27. Holloway PH (1975) The effect of surface roughness on Auger electron spectroscopy. J. of Electron Spec. and Rel. Phen. 7, 215-232.

28. Holloway PH, McGuire GE (1978) Chemical characterization of coatings by analytical techniques sensitive to the surface and near surface. Thin Sol. Films, 53, 3-18.

29. Holloway PH, Remond G, Swartz Jr. WE (1981) Interfacial Phenomena in Mineral Processing, Yarar B, Spottiswood DJ, (Eds)., New York, 93-117.

30. Holm R, Storp S (1977) ESCA studies on changes in surface composition under ion bombardment. Appl. Phys. 12, 101-112.

31. Humbert A, Hanus J (1983) An ATR analysis of surface roughness induced by electron bombardment. Surf. Sci., 129, 265-280.

32. Hunderi O, Beaglehole D (1969) On the reflectivity of rough metal surfaces. Physics Letters, 29a, 6, 335-336.

33. Joshi A, Davies LE, Palmberg PW (1975) Methods of Surface Analysis, AW Czanderna, (Ed)., Elsevier.

34. Laflamme JHG, Beaulne JM, Bourgoin Y (1979) Current polishing procedures for ore minerals, mill products, and synthetic materials in the mineralogy section, Physical Sciences Laboratory; Mineral Science Laboratory Report MRP/MSL, 79-32, 1-24.

35. Larson PE (1974) X-ray induced photoelectron and Auger spectra of Cu, CuO, Cu_2O and Cu_2S thin films. J. of Elect. Spec. and Rel. Phenom., 4, 213-218.

36. Legressus C, Massignon D, Remond G (1980) Ultra-high vacuum SEM and high spatial resolution AES in mineralogy application to sulfides. Scanning Electron Microsc. 1980; IV: 85-90.

37. Losch W (1976) An AES study of a copper-iron sulphide mineral. Surf. Sci. 60, 196-210.

38. Madden HH (1981) Chemical information from Auger electron spectroscopy. J. Vac. Sci. Technol. 18, 677-689.

39. McGuire GE (1978) Effects of ion sputtering on semiconductor surfaces. Surf. Sci., 76, 130-147.

40. McGuire GE, Holloway PH (1981) Applications of Auger Spectroscopy in Materials Analysis. In Electron Spectroscopy: Theory, Techniques, and Applications Brundle CR, Baker, AD. (Eds). 4, 1-84.

41. McIntyre NS, Zetaruk K (1977) X-ray photoelectron spectroscopic studies of iron oxides. Anal. Chem., 49, 11, 1521-1529.

42. Niehus H, Losch W (1981) ESD on metal oxides and oxygen adsorption layers: Evidence for different mechanisms in electron stimulated desorption. Surf. Sci. 111, 344-350.

43. Ohuchi F, Ogino M, Holloway PH, Pantano CG (1980) Electron beam effects during analysis of glass thin films with Auger electron spectroscopy. Surf. and Interface Anal., 2, 3, 85-90.

44. Olson RR, Palmberg PW, Hovland CT, Brady TE (1983) Applications of AES in microelectronics. In: Practical Surface Analysis by Auger and X-ray photoelectron spectroscopy, Briggs D, Seah MP, (Eds). John Wiley and Sons, 217-246.

45. Orchard AF (1978) Basic Principles of Photoelectron Spectroscopy. In: Handbook of X-ray and Ultraviolet photoelectron spectroscopy. Briggs D, (Ed). Heyden & Sons Ltd., London, 1-77.

46. Palmberg PW (1972) Use of Auger electron spectroscopy and inert gas sputtering for obtaining chemical profiles. J. Vac. Sci. Technol. 9, 160-163.

47. Porteus JO (1963) Relation between the height distribution of a rough surface and the reflectance at normal incidence. J. of the Optical Soc. of Amer. 53, 12, 1394-1402.

48. Remond G, Caye R, Gateau C, Ruzakowski P, Holloway PH (1986) Optical microreflectometry and microscopy of chalcopyrite specimens: Reflectance calculations and comparison to backscattered electron microscopy. Scanning Electron Microsc. 1986; III: 1280-1307.

49. Remond G, Giraud R, Holloway PH, Packwood RH (1984) The effect of volume and surface diffusion of impurities on the detection limit in microprobe analysis. Scanning Electron Microsc. 1984; I: 151-166.

50. Remond G, Holloway PH, Kosakevitch A, Ruzakowski P, Packwood RH, Taylor JA (1985) Electron spectroscopies and optical microreflectometry applied to the study of ZnS tarnishing in polished sulfide ore specimens. Scanning Electron Microsc. 1983; IV: 1305-1326.

51. Remond G, Picot P, Giraud R, Holloway PH, Ruzakowski P (1983) Contribution of electron spectroscopies to X-ray spectrometry applied to the geosciences. Scanning Electron Microsc. 1983; IV: 1683-1706.

52. Ruzakowski PH (1987) An Investigation of the Surface Oxidation Products formed in air on natural specimens of Chalcopyrite as a function of temperature, PhD Dissertation, Univ. of Fla., 1-198.

53. Saeki N, Shimizu R (1978) Auger study of preferential sputtering for Cu-Ni alloy sample. Jap. J. of App. Phys., 17, 1, 59-68.

54. Sanz JM, Hofmann S (1983) Auger electron and X-ray photoelectron spectroscopy studies of the oxidation of Polycrystalline Ta and Nb at room temperature and low O_2 pressure. J. of the Less-Common Metals 92, 317-327.

55. Seah MP (1983) A review of quantitative Auger electron spectroscopy. Scanning Electron Microsc. 1983; II: 521-536.

56. Seo M, Lundsen JB, Staegke RW (1975) An Auger analysis of oxide films on iron. Surf. Sci. 50, 541-552.

57. Singer KE (1979) The application of Auger depth profiling to metal-semiconductor contacts. Thin Sol. Films 57, 115-126.

58. Smith DM, Gallon TE (1974) Auger emission from solids: the estimation of backscattering effects and ionization cross sections. J. of Phys. D, App. Physics, 7, 151-161.

59. Smith T (1976) Auger electron spectroscopy and ion sputter profiles of oxides on Aluminum. Surf. Sci. 55, 601-624.

60. Sohn HY, Goel RP (1979) Principles of Roasting. Minerals Sci. Eng. 11, 3 137-153.

61. Storp S, Holm R (1979) ESCA investigations of ion beam effects on surfaces. J. of Electron Spec. and Rel. Phen. 16, 183-193.

62. Thomas MT, Petersen DA, Hartley JN, Freeman HD (1981) Interfacial Phenomena in Mineral Processing, Yarar B, Spottiswood DJ, (Eds.), Engineering Foundation, New York, 33-61.

63. Tompkins HG (1987) Modelling the effect of ion mixing and surface roughening on depth profiles. Surf. and Int. Anal., 10, 105-109.

64. Wehner GK (1975) In: Methods of Surface Analysis, Czanderna AW, (Ed). Am. Elsevier, New York, 1-37.

Discussion with Reviewers

M.T. Thomas: Has this work led to changes and improvements to mineral processing to improve Cu recovery?

Authors: The work reported in this paper has led to better characterization of the minerals contained within an ore. These data have directly affected the procedure used for treating and grinding the ore in preparation for mineral recovery. Other surface studies along with these have been used to predict variations in recovery procedures which have led to enhanced recovery. Therefore the answer to the question is yes, but not based exclusively on the present paper nor exclusively on the present authors.

D.W. Schowengerdt: Did you check the chemical state of Fe using XPS in the regions where you identified Fe_2O_3 and Fe_3O_4 by AES? Were the XPS results consistent with your interpretation of the AES peak splittings?

Authors: Yes this was checked with XPS, and yes the two data sets agreed with one another.

D.W. Schowengerdt: How do you know that the sputtering removed FeOOH to expose Fe_3O_4 rather than converting one into the other by ion-induced processes?

Authors: While we did not perform the experiment of sputtering/bulk FeOOH to show it would or would not reduce to Fe_3O_4 under our ion bombardment conditions, the amount of Fe_3O_4 observed was too much to derive strictly from ion conversion of FeOOH. Thus both FeOOH and Fe_3O_4 must initially have been present.

M.F. Hochella, Jr.: Can the authors be more specific on how their findings can be used to further understand and develop sulfide mineral processing or benefication? What is the significance of understanding the surface alteration of sulfides up to 300°C within this context?

Authors: For the first part of this question, please refer to the answer given above in response to M.T. Thomas. With respect to the second half we had two purposes. First to begin investigating the ability to do an accelerated ageing of minerals which might experience "weathering" after partial completion of the recovery process. Second, we also wanted to see if we could simulate segregation and oxidation over geologic time by accelerated ageing. These questions are so broad that one study cannot answer them, but we were successful in demonstrating that segregation could be observed by "accelerated ageing".